Supplementary Data

Experimental mapping of DNA duplex shape enabled by global lineshape analyses of a nucleotide-independent nitroxide probe

Yuan Ding, Xiaojun Zhang, Kenneth W. Tham and Peter Z. Qin*

Departments of Chemistry, University of Southern California, Los Angeles, CA 90089

*Corresponding author: LJS 251, 840 Downey Way, Los Angeles, CA 90089. Tel: (213) 821-2461; Fax: (213) 740-0930; Email: pzq@usc.edu

Table S1: DNA oligonucleotides used in this study.

Sequence name	Sequence	Extinction coefficient ($M^{-1} \cdot cm^{-1}$)
BAX-labeled strand	5′-T C A C A A G T T A g A G A C A A G C C T-3′ p p p p p p p p p p p p p p p p p p p p	211,400
BAX-complementary strand	5′-biotin-A G G C T T G T C T c T A A C T T G T G A-3′ p p p p p p p p p p p p p p p p p p p p p p	197,700
p21-labeled strand	5′-G A A C A T G T C C C A A C A T G T T G-3′ p p p p p p p p p p p p p p p p p p p p	194,900
p21-complementary strand	5′-biotin-C A A C A T G T T G G G A C A T G T T C-3′ p p p p p p p p p p p p p p p p p p p p p p	192,700

Table S2: Key for spectral number in the P-matrix.

Spectral Number	DNA Site	P_{TEMPOL}	di-nucleotide step
1	BAX_9	0.575	TpT
2	BAX_15	0.555	ApC
3	p21_6	0.554	ApT
4	BAX_4	0.543	ApC
5	p21_16	0.540	ApT
6	p21_8	0.535	GpT
7	p21_11	0.531	CpC
8	p21_9	0.530	TpC
9	BAX_13	0.529	ApG
10	BAX_11	0.526	ApG
11	BAX_8	0.523	GpT
12	p21_4	0.520	ApC
13	p21_14	0.520	ApC
14	BAX_6	0.517	ApA
15	BAX_10	0.515	TpA
16	p21_7	0.514	TpG
17	p21_10	0.514	CpC
18	p21_18	0.511	GpT
19	p21_13	0.510	ApA
20	BAX_7	0.509	ApG
21	BAX_14	0.504	GpA
22	p21_5	0.502	CpA
23	BAX_18	0.502	ApG
24	BAX_17	0.500	ApA
25	p21_17	0.499	TpG
26	p21_12	0.495	CpA
27	BAX_12	0.492	GpA
28	BAX_19	0.491	GpC
29	BAX_16	0.488	CpA
30	BAX_5	0.484	CpA
31	p21_15	0.472	CpA

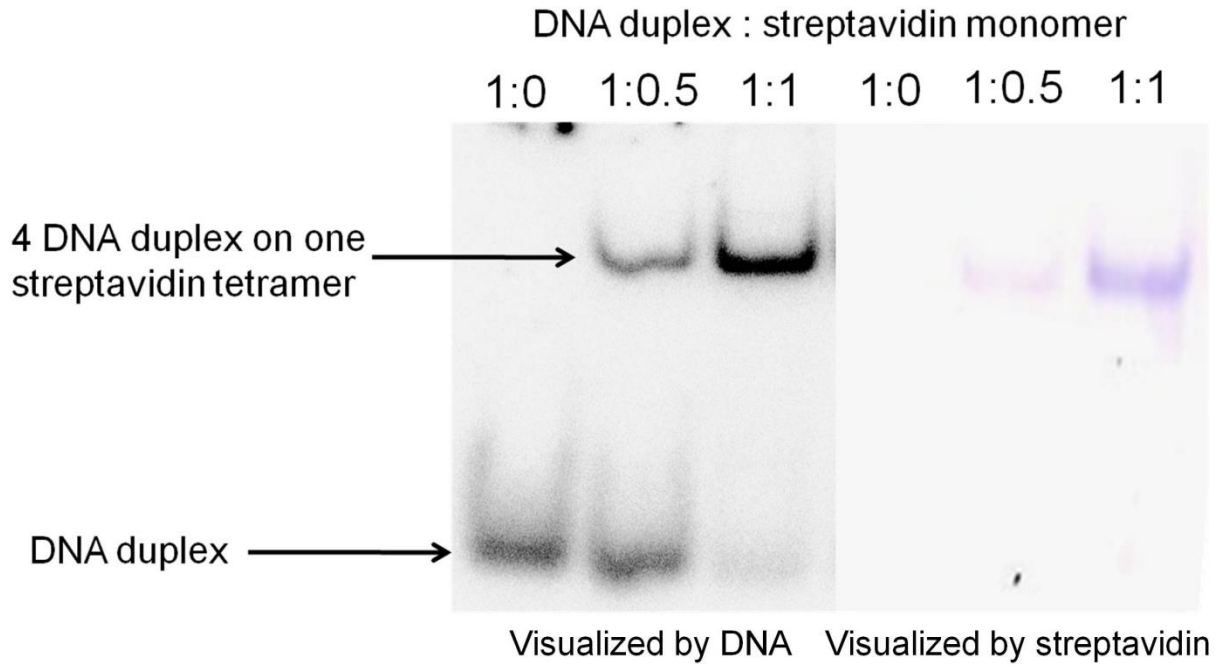

Figure S1: DNA tethering to streptavidin examined by a native gel shift assay. In each sample, 40 μM of DNA duplex was mixed with traced amount of ^{32}P labeled DNA duplex, then incubated with streptavidin in 50 mM HEPES (pH 7.5), 100 mM NaCl, and 5 mM $MgCl_2$. The samples were loaded onto a 8% native polyacrylamide gel that was prepared in a buffer containing 50 mM HEPES, pH 7.5, 100 mM NaCl, 5 mM $MgCl_2$, and 89 mM boric acid. The gel was run in the same buffer at 4°C, and was visualized by both phosphorimaging (left) and Coomassie Blue staining (right). The data show that with increasing concentration of streptavidin, one DNA-streptavidin complex is formed. This species was assigned as DNA tethered to a streptavidin tetramer, as previous studies reported that streptavidin exists as tetramer when bound to biotin under similar conditions (1).

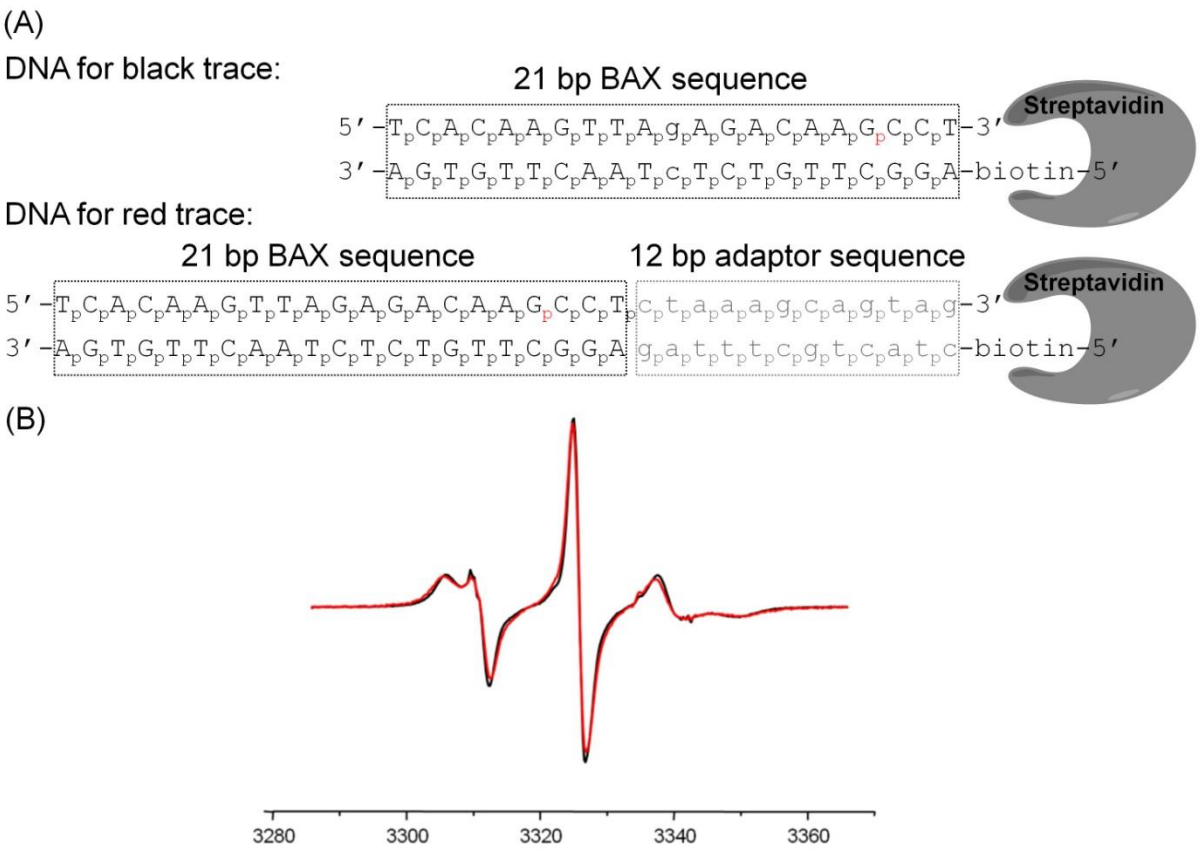

Figure S2: Examining spectral effects due to altering the relative positioning between the R5a labeling site and streptavidin. Two EPR spectra of streptavidin tethered BAX_19 are shown. The black trace was obtained with 21-bp BAX duplex tethered directly to streptavidin (panel (A), top), in which case the R5a label at the BAX_19 site was closest to the tethering point and expected to have the highest probability to contact streptavidin. The red trace was obtained with a 12 base-pair adaptor sequence (gray, lower case) placed in between the BAX duplex and streptavidin (panel (A) bottom), which placed the BAX_19 site further away from the streptavidin and was expected to eliminate/reduce R5a-streptavidin contacts. The two spectra show identical lineshape, with a pair-wise Pearson coefficient of 0.993. This indicates that R5a spectrum was not affected upon changing the relative location between R5a and streptavidin, indicating a lack of direct R5a-streptavidin contacts.

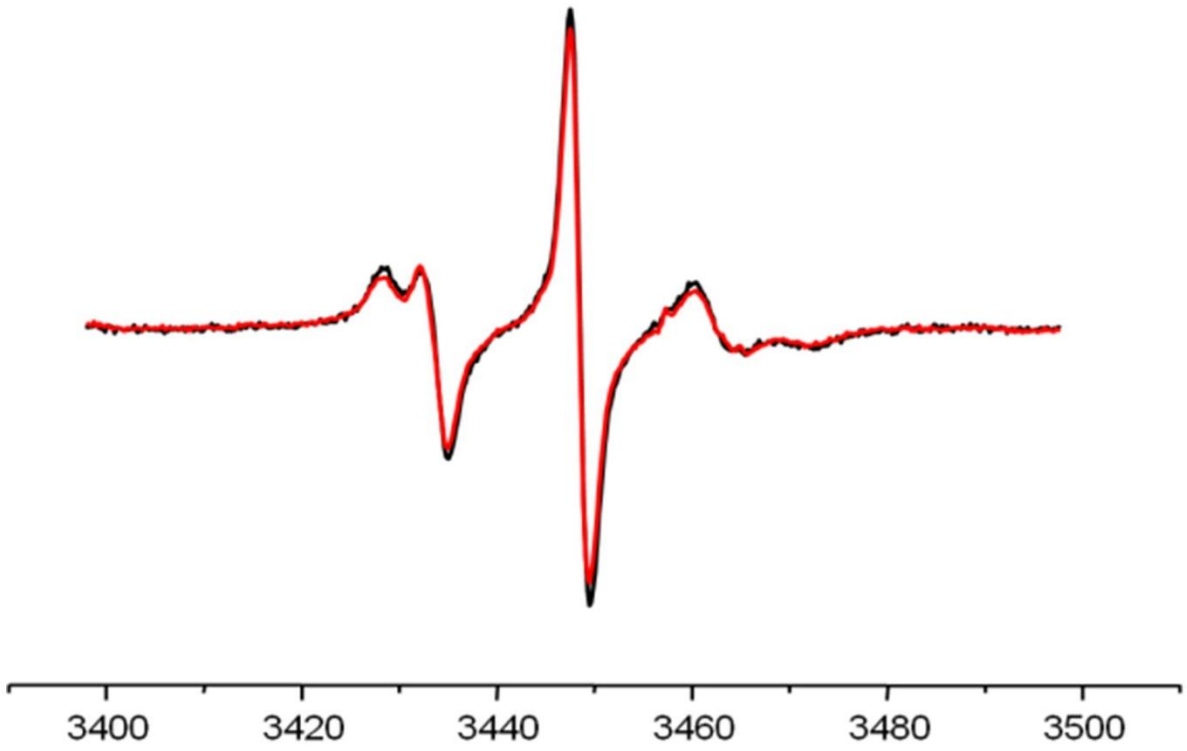

Figure S3: Assessing potential inter-molecular di-polar interaction in the streptavidin tethered DNAs. Two streptavidin tethered p21_18 spectra were compared. The black trace was obtained from a sample in which 100% of the p21 duplex was labeled with R5a, while the red trace was obtained in which 20% of the p21 duplex was labeled. No broadening was observed when comparing the 100% labeled sample to that of 20% labeled. The pair-wise P was calculated to be 0.999. This indicates that inter-molecular di-polar interaction minimally affects the observed spectral lineshape under our experiment conditions.

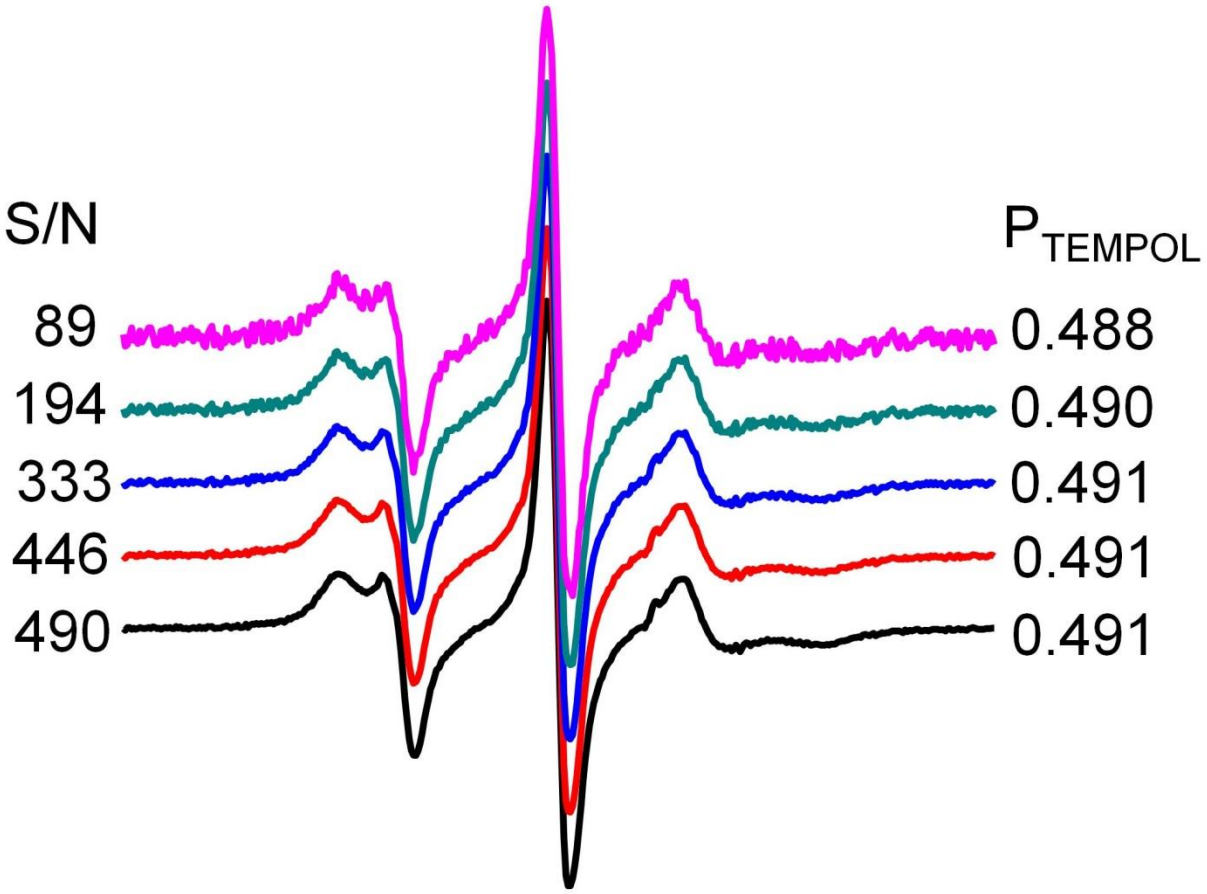

Figure S4: Examining the impact of noise on Pearson coefficient. Various amount of random noise was added to the measured BAX_19 spectrum, and then the P_{TEMPOL} values were computed. For signal-to-noise (S/N) ratio > 300, no change in P_{TEMPOL} was observed.

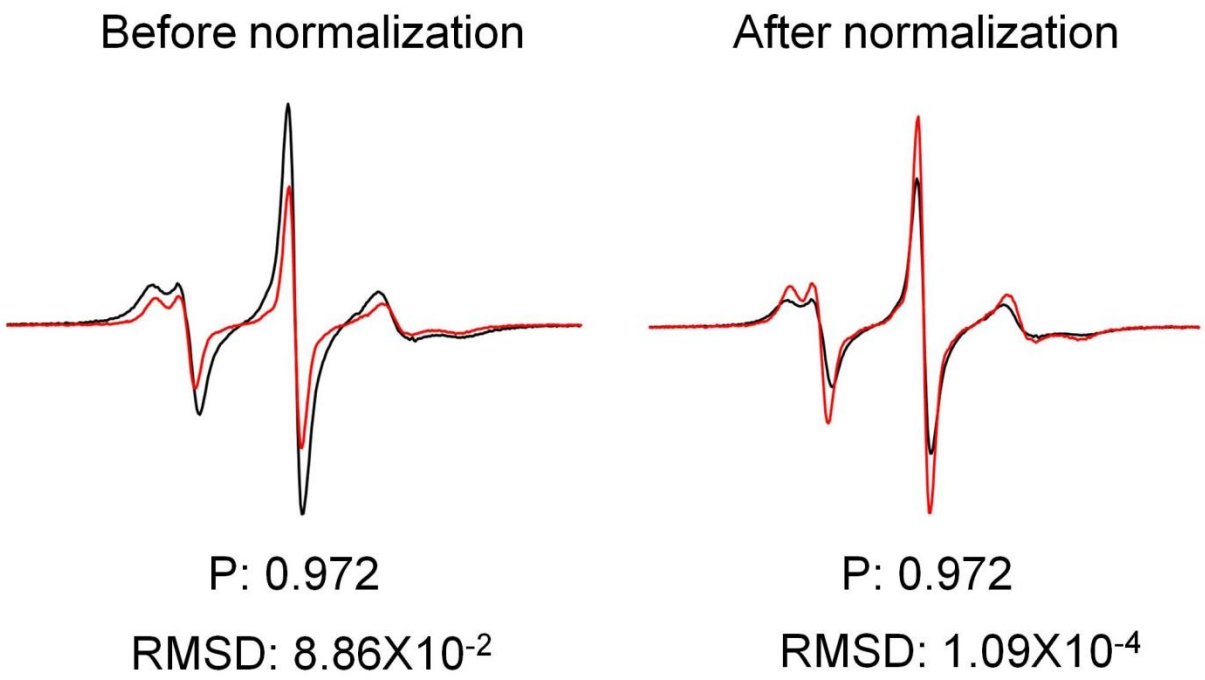

Figure S5: Sensitivity of Pearson coefficient and RMSD on spectra normalization. Two spectra plotted here are BAX_17 (black trace) and BAX_10 (red trace) for both before and after normalization. P(BAX_17/BAX_10) remains unchanged upon spectral normalization, while the RMSD value changes drastically.

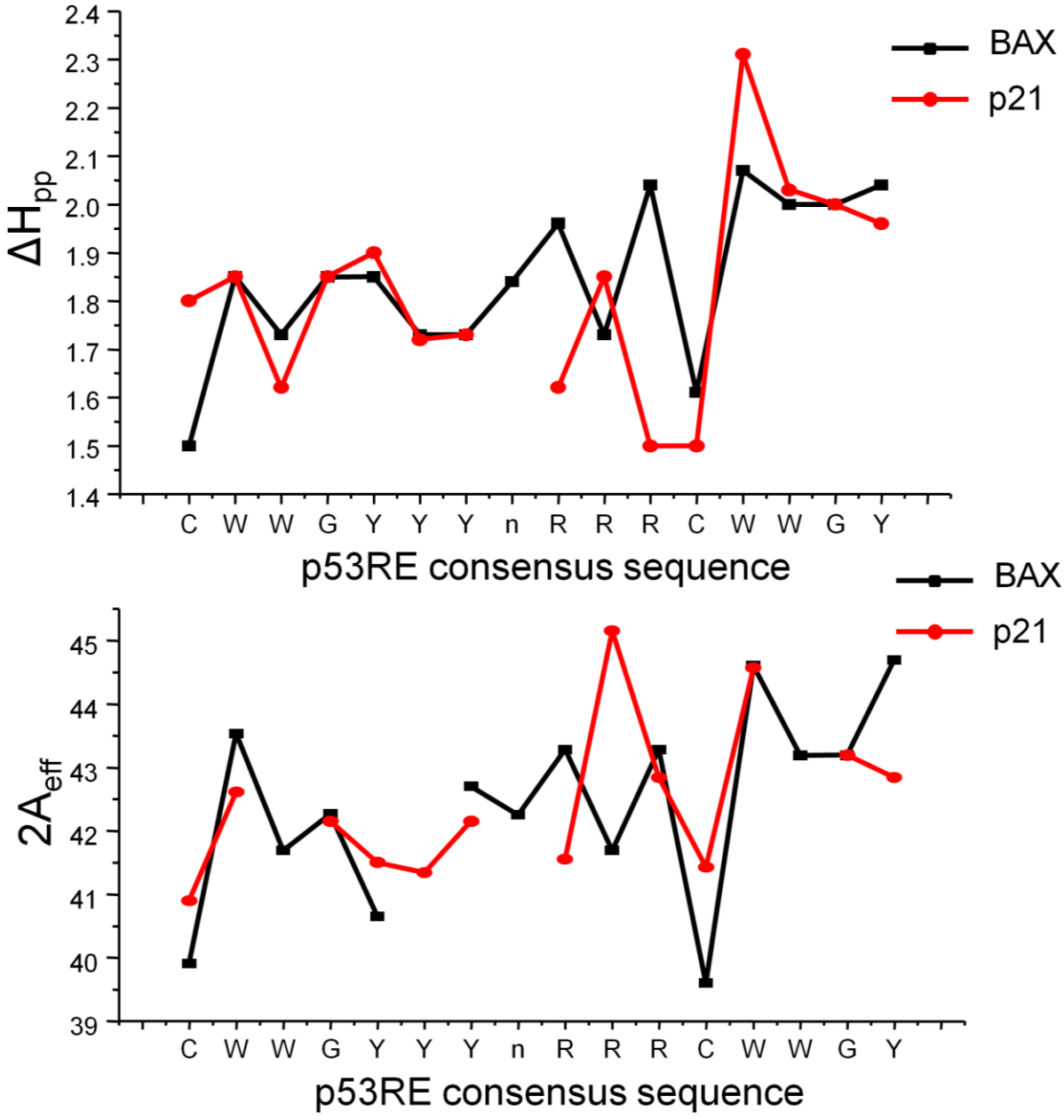

Figure S6: Map of central line width (ΔH_{pp}) (top panel) and effective hyperfine splitting ($2A_{eff}$) (bottom panel) in the BAX (black) and p21 (red) duplexes.

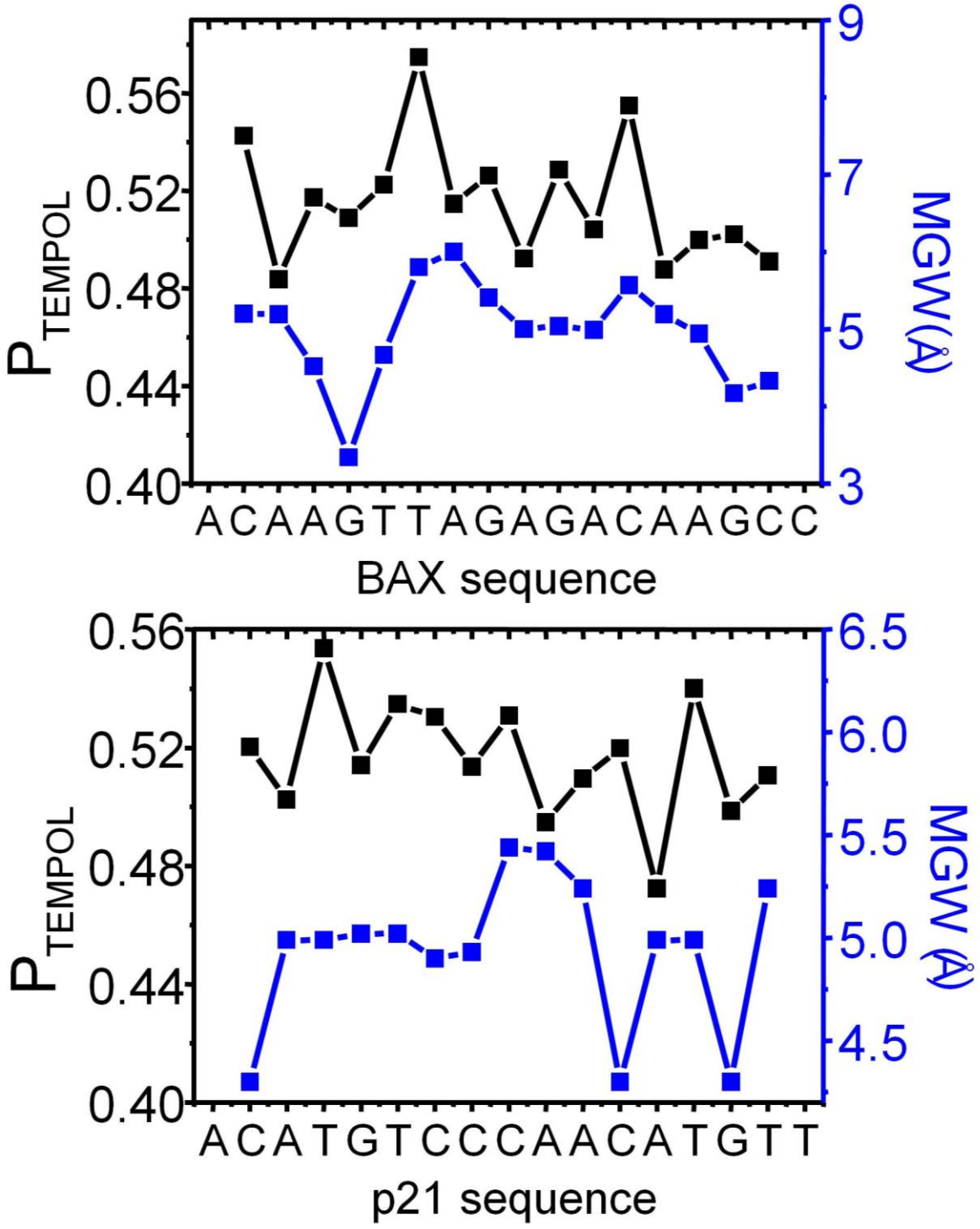

Figure S7: Comparisons between maps of P_{TEMPOL} (black) and minor groove width (MGW, blue) for BAX (top panel) and p21 (bottom panel). P_{TEMPOL} value was aligned to the MGW value for the base-pair 3' of the spin label. Pearson coefficients between the two maps were 0.419 and 0.007, respectively, for BAX and p21.

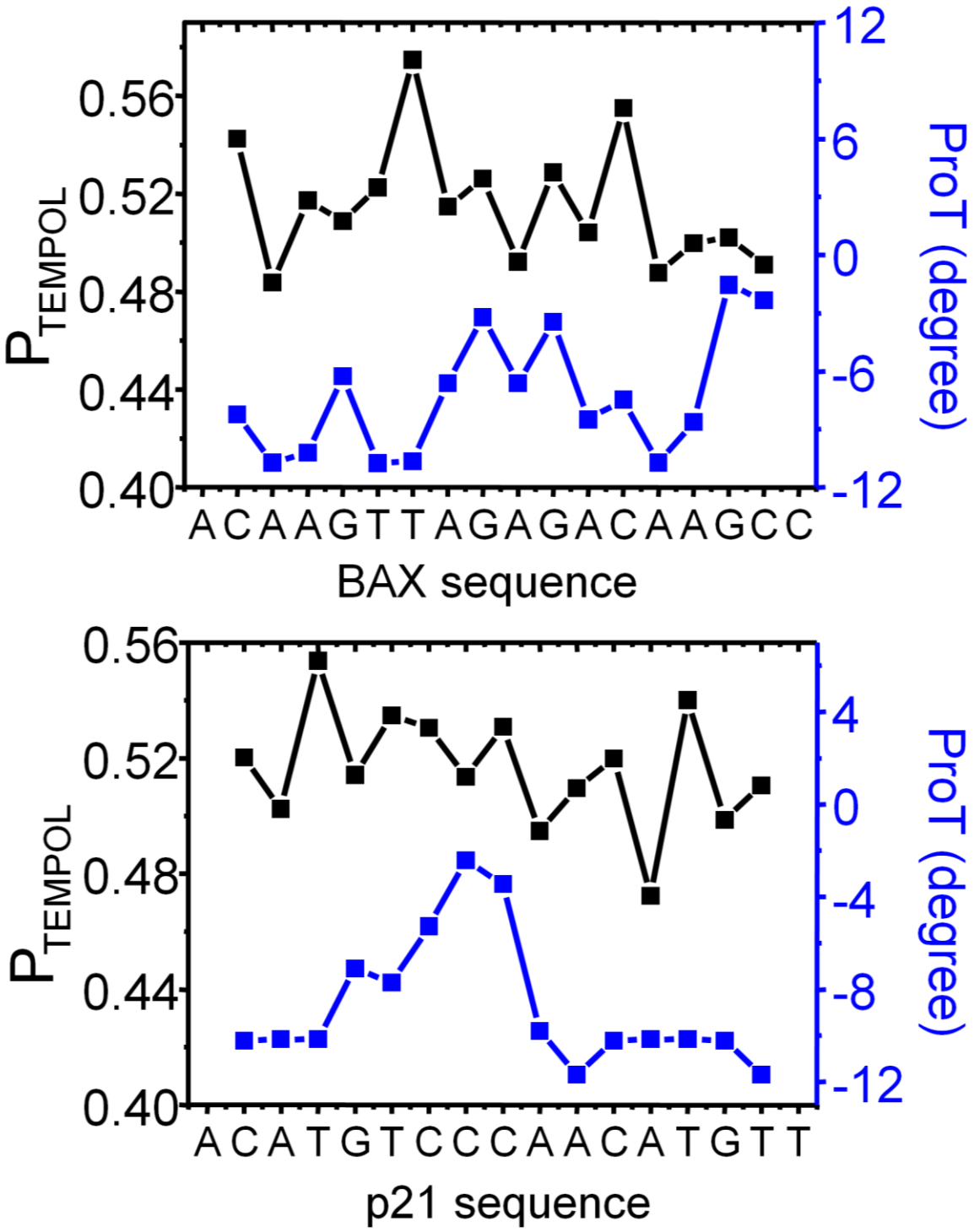

Figure S8: Comparisons between maps of P_{TEMPOL} (black) and propeller twist (ProT, blue) for BAX (top panel) and p21 (bottom panel). P_{TEMPOL} value was aligned with the ProT value for the base-pair 3' of the spin label. Pearson coefficients between the two maps were -0.124 and 0.237, respectively, for BAX and p21.

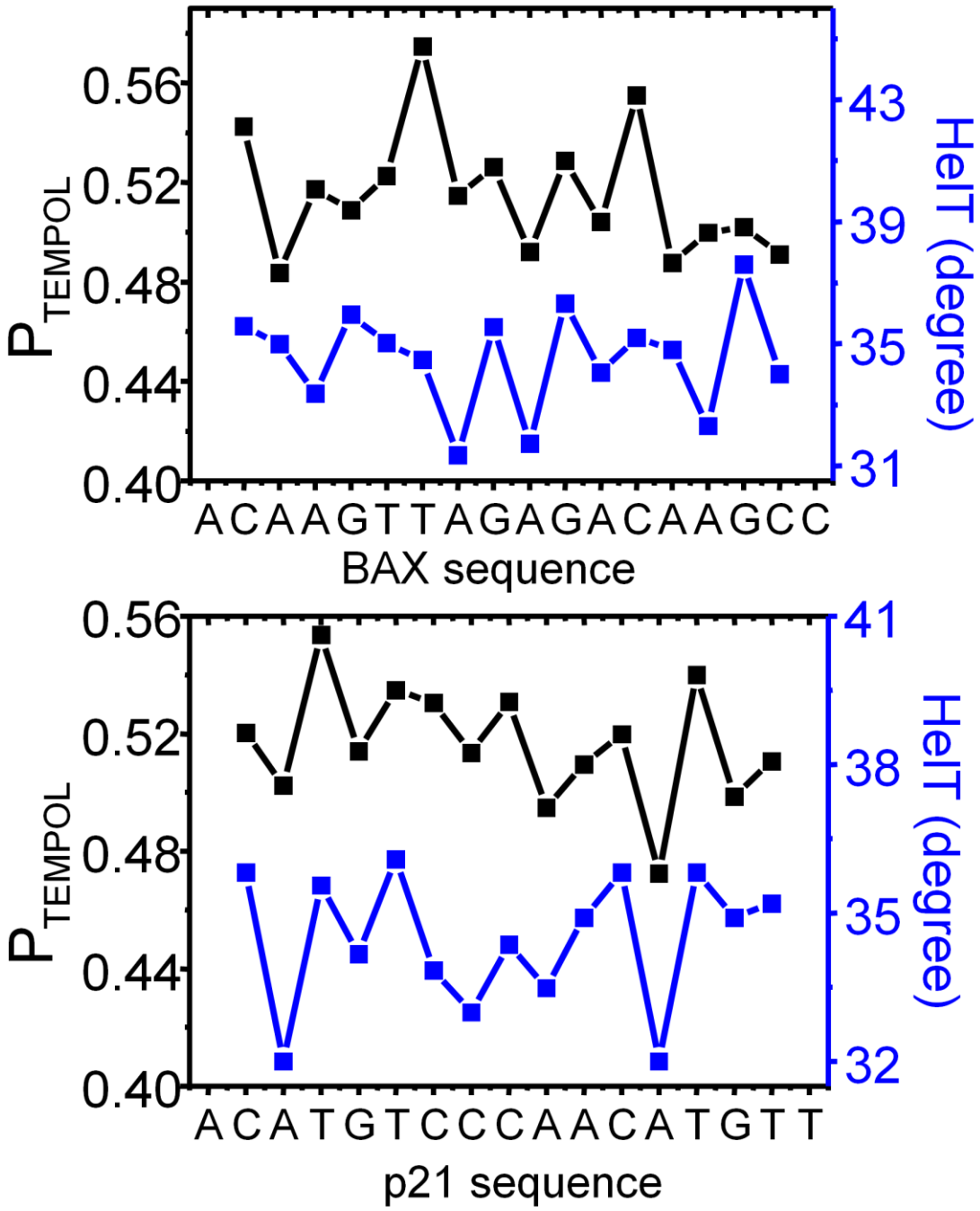

Figure S9: Comparisons between maps of P_{TEMPOL} (black) and helical twist (HelT, blue) for BAX (top panel) and p21 (bottom panel). P_{TEMPOL} value was aligned to the HelT value of the base-pair step 3' of the spin-labeled phosphate. Pearson coefficients between the two maps were 0.210 and 0.664, respectively, for BAX and p21. Note that correlation between the predicted map of Roll and HelT is high for p21 (0.591) but low for BAX (0.035). As P_{TEMPOL} shows high correlation to Roll in both BAX and p21, correlation between P_{TEMPOL}/HelT can only be high for p21.

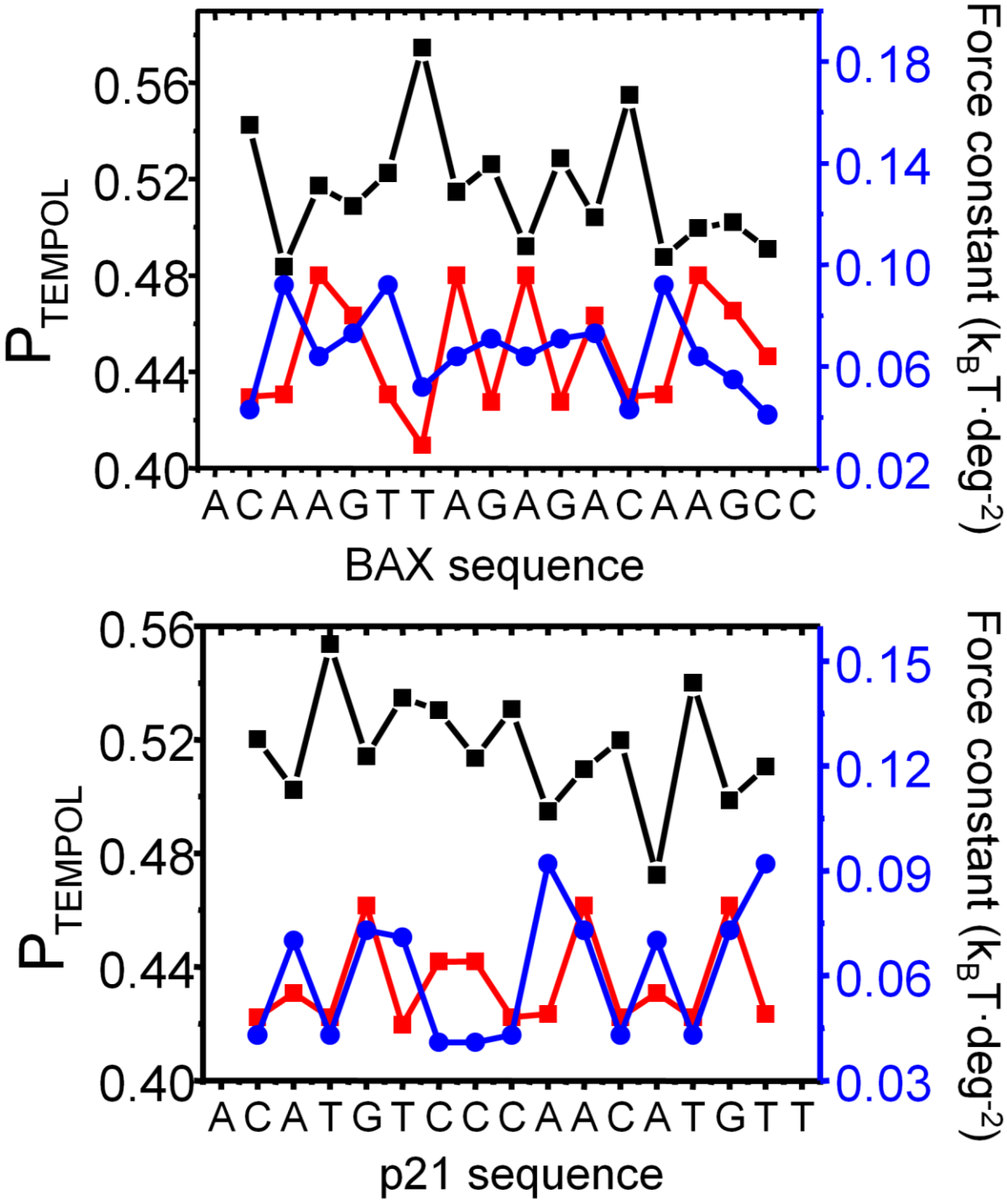

Figure S10: Comparisons between maps of P_{TEMPOL} (black), Roll-Roll force constant (red), and HelT-HelT force constant (blue) for BAX (top panel) and p21 (bottom panel). The force constants were obtained from reference (2). P_{TEMPOL} value was aligned to the force constant for the base-pair step 3' of the spin-labeled phosphate. For BAX, Pearson coefficients were -0.517 and -0.456, respectively, for P_{TEMPOL}/Roll-Roll and P_{TEMPOL}/HelT-HelT. For p21, they were -0.314 and -0.599, respectively.

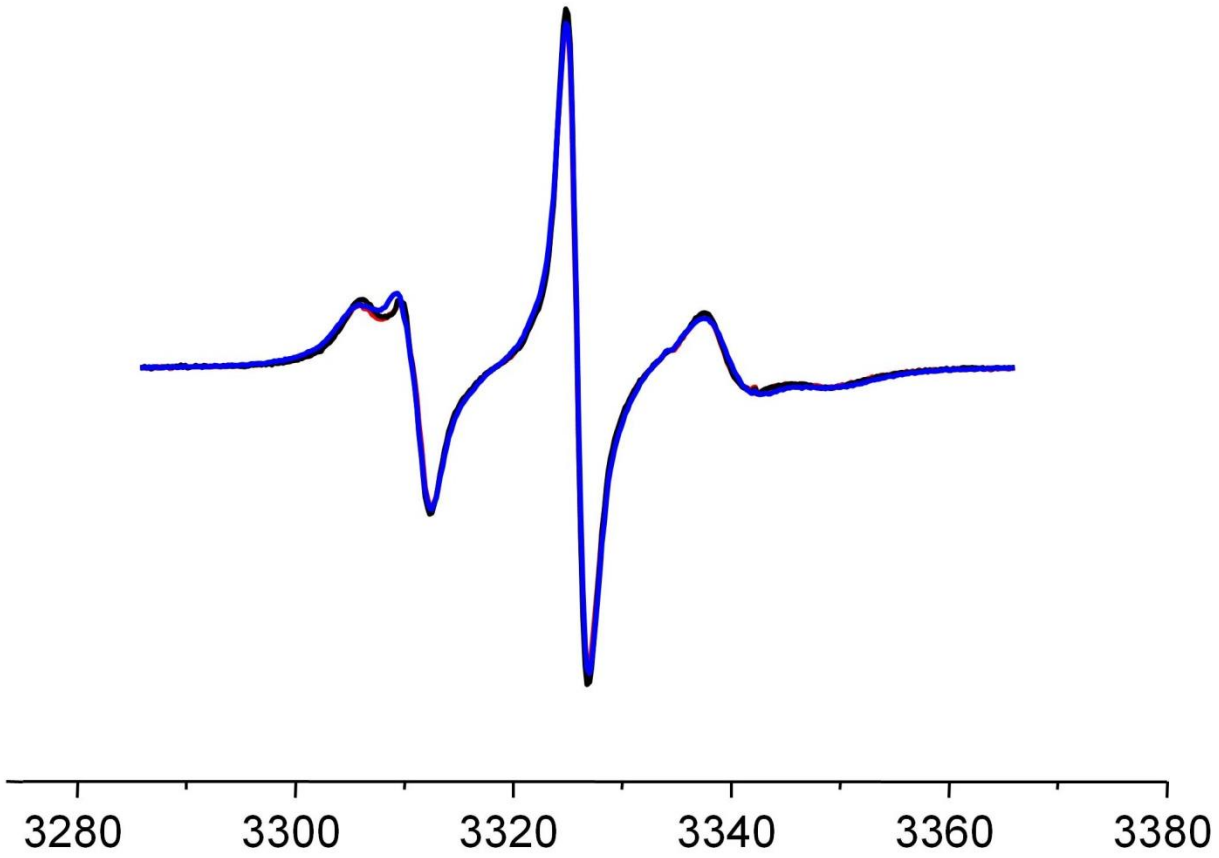

Figure S11: Overlay of spectra that showed a high degree of similarity in the P-matrix (main text Figure 6). Black: spectrum 23 (BAX_18); Red: spectrum 24 (BAX_17); Blue: spectrum 25 (p21_17). The pair-wise P values among these three spectra were P(BAX_17/BAX_18): 0.999; P(BAX_18/p21_17): 0.998; and P(BAX_17/p21_17): 0.998.

References:

1. Sano, T. and Cantor, C.R. (1995) Intersubunit contacts made by tryptophan 120 with biotin are essential for both strong biotin binding and biotin-induced tighter subunit association of streptavidin. *Proc Natl Acad Sci U S A*, **92**, 3180-3184.
2. Olson, W.K., Gorin, A.A., Lu, X.J., Hock, L.M. and Zhurkin, V.B. (1998) DNA sequence-dependent deformability deduced from protein-DNA crystal complexes. *Proc Natl Acad Sci U S A*, **95**, 11163-11168.